Journal of Non-Crystalline Solids 482 (2018) 147–153

Contents lists available at ScienceDirect

Journal of Non-Crystalline Solids

journal homepage: www.elsevier.com/locate/jnoncrysol

BaF_2 modified Cr^{3+}/Ho^{3+} co-doped germanate glass for efficient 2.0 μm fiber lasers

X.L. Yang, W.C. Wang, Q.Y. Zhang*

State Key Laboratory of Luminescent Materials and Devices, Institute of Optical Communication Materials, South China University of Technology, Guangzhou 510641, China

ARTICLE INFO

Keywords:
Cr^{3+}/Ho^{3+} co-doped
Germanate glasses
BaF_2 modifiers
2.0 μm fiber laser

ABSTRACT

The influence of BaF_2 on the physical and spectroscopic properties of Cr^{3+}/Ho^{3+} co-doped germanate glass is investigated systematically by differential scanning calorimeter, excitation and emission spectra, as well as dynamic decay lifetime. The intense and broad absorption band of Cr^{3+} provides a selective pump scheme for obtaining an efficient 2.0 μm emission of Ho^{3+}, the OH^- absorption coefficient, on the other hand, is decreased as low as 1.08 cm^{-1}, which both highly conducive to obtain an intense 2.0 μm emission of Ho^{3+}. In addition, the crystal-field parameter D_q/B of Cr^{3+}-doped glasses is also calculated to study the influence of BaF_2 on the local environment of activators and sensitizers. Further theoretic calculation shows that the largest absorption and emission cross-sections of Ho^{3+} near 2.0 μm are as high as 4.6 and 5.2 ($\times 10^{-21}$ cm^2) in the 10 mol% BaF_2 modified Cr^{3+}/Ho^{3+} co-doped glass and the maximum energy transfer efficiency from Cr^{3+} to Ho^{3+} is about 42.5%. All results suggest that this BaF_2 modified Cr^{3+}/Ho^{3+} co-doped glass is very suitable for a high-efficient 2.0 μm fiber lasers with flexible pump sources.

1. Introduction

In recent years, Ho^{3+} ion has gained lots of significant interest for the development of 2.0 μm solid-state fiber lasers due to its relatively higher stimulated emission cross-section, longer decay lifetime and longer laser wavelength [1,2]. However, Ho^{3+} ion suffers from a certain limitation of non-absorbing commercially available 808 nm or 980 nm laser diodes (LDs), a common approach to solving this problem is employing a series of appropriate rare-earth ion sensitizers to enhance the 2.0 μm emission of Ho^{3+}, such as Yb^{3+} [3], Tm^{3+} [4], Er^{3+} [5], and Nd^{3+} [6]. Unfortunately, the sensitizing effect of current rare-earth ions is strictly defined by their narrow excitation and emission bands [7]. As an excellent sensitizer, the *d-d* transitions of chromium ion are intensively investigated [8–13]. For example, in our previous work [7], the various valance of chromium (Cr^{3+}, Cr^{4+}, Cr^{6+}) can be detected by the absorption spectra from the fluoride-sulfophosphate glasses [9]. Besides that, the Cr^{3+} and Cr^{6+} instead of Cr^{4+} have been observed in the germanate glasses [8]. It should be noted that only Cr^{3+} is beneficial for achieving efficient energy transfer process between Cr^{3+} and Ho^{3+} or Tm^{3+} ions [7,8]. The efficient 2.0 μm fluorescence has been obtained in the Ho^{3+}-doped glass sensitized by Cr^{3+}, an interesting finding is that the intense and broad absorption band of Cr^{3+} provides a selective pump scheme for obtaining an intense 2.0 μm emission of Ho^{3+} [7]. In order to explore flexible pump sources and improve the pumping efficiency for Ho^{3+}, more efforts should be performed to further study the sensitizing mechanism between Cr^{3+} and Ho^{3+} and improve their energy transfer efficiency.

On the other hand, germanate glass has been considered as a proper laser glass host for Ho^{3+} ion, which owns a lower maximum phonon energy, outstanding chemical stability, thermal stability, and excellent solubility for the rare-earth ions [14–17]. Nevertheless, it is recognized that an oxygen bridging ^4Ge and ^6Ge is forming a hydrogen bond with an OH^- group in germanate glass, which constitutes an impurity quenching center for mid-infrared luminescence [18–20]. The introduction of proper amounts of fluorides into germanate glass can transform the glass structure and suppress the OH^- groups simultaneously [21]. In addition, the local environment of activators and sensitizers can be influenced by the incorporation of BaF_2, which may produce a higher pump efficiency for achieving an efficient energy transfer process from Cr^{3+} to Ho^{3+}.

Based on the above research backgrounds and reasons, this paper creatively studies the BaF_2 modified Cr^{3+}/Ho^{3+} co-doped germanate glass for efficient 2.0 μm fiber lasers. The influence of BaF_2 on the physical and spectroscopic properties of Cr^{3+}/Ho^{3+} co-doped germanate glass was investigated systematically by differential scanning calorimeter, excitation and emission spectra, as well as dynamic decay

* Corresponding author.
E-mail address: qyzhang@scut.edu.cn (Q.Y. Zhang).

https://doi.org/10.1016/j.jnoncrysol.2017.12.031
Received 31 October 2017; Received in revised form 15 December 2017; Accepted 16 December 2017
Available online 28 December 2017

lifetime. A key finding is that the excitation spectra of Cr^{3+} can be easily tailored by the incorporation of BaF_2, which ultimately makes a higher pump efficiency for achieving an efficient energy transfer process from Cr^{3+} to Ho^{3+}. In addition, the energy transfer efficiency from Cr^{3+} to Ho^{3+} is improved as high as 42.5%. All results suggest that this BaF_2 modified Cr^{3+}/Ho^{3+} co-doped glass is very suitable for a high-efficient 2.0 μm fiber lasers with flexible pump sources.

2. Experiment

The glass compositions were (20-*x*)BaO-(14.9-*y*)Ga_2O_3-65GeO_2-*x*BaF_2-0.1Cr_2O_3-*y*Ho_2O_3 (x = 0, 5, 10, 15, 20; y = 0, marked as BGG:Cr^{3+}; x = 0, 5, 10, 15, 20; y = 1.0, marked as BGG:Cr^{3+}/Ho^{3+}, respectively). In addition, two glass samples 20BaO-15Ga_2O_3-65GeO_2 (BGG), 20BaO-14Ga_2O_3-65GeO_2-1Ho_2O_3 (BGG:Ho^{3+}) were prepared as comparisons. The starting materials were extra pure anhydrous reagents of GeO_2 (Civi-Chem 99.999%), Ga_2O_3 (Aladdin, 99.99%), $BaCO_3$ (Aladdin, 99.99%), BaF_2 (Aladdin, 99.99%), Cr_2O_3 (Aladdin, 99.95%), and Ho_2O_3 (Aladdin, 99.99%). A batch of 15 g starting materials was completely weighed and mixed. Afterwards, the mixtures were melted in an alumina crucible covered by an alumina lid inside an electric furnace at 1350 °C for 30 min in air. Then the melts were poured into a preheated stainless steel mold and annealed at 400 °C for 2 h. The annealed specimens were well cut and polished into about 1.5 mm thickness for subsequent measurements.

Differential scanning calorimeter (STA449C/3/MFC, Germany) was conducted with N_2 as protected atmosphere at a heating rate of 10 K/min. The transmission spectra were acquired on a Vector-33 FTIR spectrometer (Bruker, Switzerland). Near-infrared (800–1700 nm) emission and excitation spectra as well as the fluorescence decay curves were measured on FLS-920 spectrometer (Edinburgh Instruments Ltd.) using a 450 W Xe lamp at 619 nm or a 150 W microsecond pulsed lamp as excitation sources, respectively, a liquid nitrogen cooled R5509-72 photomultiplier (PMT) as the detector. Photoluminescence spectra were measured on a Triax 320 type spectrofluorometer (Jobin-Yvon Corp.) fitted with an InGaAs detector (900–1500 nm) and a PbSe detector (1800–2300 nm) using an 808 nm laser diode (LD) as the irradiation source. The luminescence decay curves for 2.0 μm emission were captured by a Tektronix TDS 3012c Digital Phosphor Oscilloscope with pulsed 808 nm LD. All the measurements were carried out at room temperature.

3. Results and discussions

Glass forming region (GFR) is the basis of fabricating the barium gallo-germanate glass, which has been experimentally delivered in [22], as marked in Fig. 1(a) with blue lines. Nevertheless, many superfluous endeavors have been carried out to discover their experimental GFR and there is a critical point in finding the GFR *via* a more efficient way. In our previous report [23], the GFR was predicted for selecting an optimal glass composition. The calculated GFR is found at around eutectic points (T_1, T_2, T_3), as shown in Fig. 1(a) with red lines, these points are correspondingly achieved from the points e_1, e_2, e_3 that are obtained on the basis of the related binary phase diagram [23]. In comparison with the calculated and the experimental GFR [22], an apparent difference comes from the discrepancies of the referred binary phase diagram data and the preparation condition [23]. The considered point 1 (composition: 20BaO-15Ga_2O_3-65GeO_2) [21] is located at both the experimental [22] and the calculated GFR, which basically signifies the glass stability of point 1. When the proper amount of BaF_2 is added in substitution of BaO, the modified glasses also keep good stability by the common melt-quenching preparation. In order to evaluate glass thermal stability, DSC curves are exploited to determine the glass characteristic temperatures such as the glass transition temperature T_g, glass crystallization temperature T_x and the criterion ΔT ($\Delta T = T_x - T_g$) [14]. Fig. 2 displays the DSC spectra of BGG:Cr^{3+} with

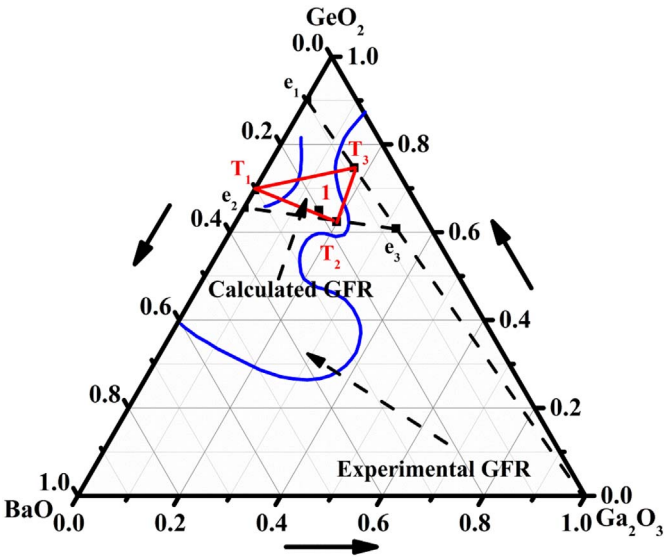

Fig. 1. The experimental and calculated GFR of BGG glass. (For interpretation of the references to color in this figure, the reader is referred to the web version of this article.)

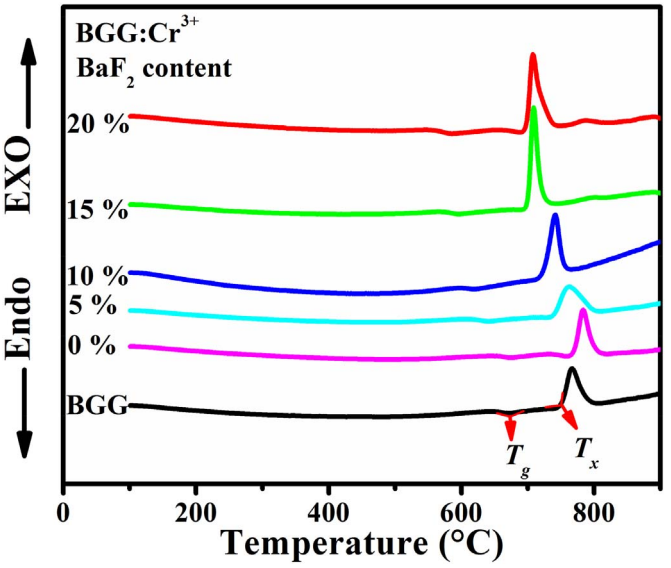

Fig. 2. DSC spectra of BGG and BGG:Cr^{3+} glasses with different BaF_2 contents.

Table 1
The typical temperatures (T_g, T_x, ΔT) of BGG and BGG:Cr^{3+} glasses with different BaF_2 contents.

Glass typical temperature	BGG	0%	5%	10%	15%	20%
T_g (°C)	648	643	619	592	569	556
T_x (°C)	738	762	734	715	694	690
ΔT (°C)	90	119	115	123	125	134

different amounts of BaF_2, the detailed values are shown in Table 1. Here, the declines of T_g and T_x are ascribed to the more loosely packed glass network with increasing BaF_2 content [21]. Besides, it is informed that ΔT values for all the Cr^{3+} doped samples are above 100 °C, confirming excellent thermal stability against crystallization [24,25]. Table 2 exhibits the basic physical properties of Cr^{3+} or/and Ho^{3+} doped glasses with different BaF_2 amounts. The more loosely packed glass network is inferred from the declines of the density and refractive index with increasing BaF_2 contents [21,26].

Fig. 3(a) depicts typical absorption bands of Ho^{3+} ions, which are

Table 2
The basic physical properties of Cr^{3+} or/and Ho^{3+} doped glasses with different BaF_2 contents.

Glass	Density (g·cm^{-3})	Average molar weight (g·mol^{-1})	Calculated Cr^{3+} (Ho^{3+}) concentration (10^{20} cm^{-3})	Refractive index @ 633 nm	α_{OH}^- (cm^{-1})	N_{OH}^- (10^{18} cm^{-3})
0% (Cr^{3+})	4.631	135.5	0.411	1.710	4.04	49.50
5%	4.623	134.4	0.410	1.703	3.45	42.26
10%	4.612	133.3	0.409	1.688	2.71	33.21
15%	4.577	132.2	0.406	1.680	1.68	20.51
20%	4.557	131.1	0.404	1.668	1.17	14.36
0% (Cr^{3+}/Ho^{3+})	4.680	137.5	4.096	1.712	3.88	47.62
5%	4.675	136.4	4.092	1.709	3.33	40.82
10%	4.648	135.3	4.068	1.689	2.07	25.39
15%	4.595	134.2	4.022	1.683	1.37	16.79
20%	4.566	133.1	3.996	1.669	1.08	13.28

respectively contributed to the transitions from the ground level of $^5I_8$ to the excited state levels of $^5I_7$, $^5I_6$, $^5I_5$, $^5F_5$, ($^5S_2$, $^5F_4$), ($^5F_2$, $^3K_8$, $^5F_3$), and ($^5F_1$, $^5G_6$) [7]. The wide absorption bands of Cr^{3+} ion are apparently centered at 350, 440, and 640 nm. Bands around 440 nm and 640 nm are contributed to the transitions from the $^4A_2$ ground state to $^4T_1$ and $^4T_2$ excited states of Cr^{3+} and 350 nm band is ascribed to Cr^{6+}, respectively [7]. The lack of 1200 nm band in the absorption spectra indicates no evidence of Cr^{4+} in these germanate glasses [8]. Therefore, in this case, Cr^{3+} is the main valance of chromium ion and a huge potential advantage of multi-wavelength pump scheme is supported by the whole broad bands around 330–850 nm of chromium ions. Fig. 3(b) donates the transmission spectra around 1700–3200 nm of Cr^{3+}-doped samples with different BaF_2 contents. The OH^- absorption coefficient (α_{OH}^-) and concentration (N_{OH}^-) of BGG:Cr^{3+} with different BaF_2 contents are calculated [26] and displayed in Table 2. The OH^- coefficient is lowered as low as 1.08 cm^{-1} after introducing 20% BaF_2 due to the chemical reaction of Ge-OH and BaF_2 [18], which is lower than that of some germanate glass (3.05 cm^{-1}) [27]. The inset represents the photograph of the samples, the visually green intensity of samples is distinctly faded when the amount of BaF_2 increases at 15%. The color of samples changes in relation to the absorption band-shift of Cr^{3+} in Fig. 3(c), the zoomed absorption band of Cr^{3+}:$^4T_2$ shows a blue shift as the amount of BaF_2 reaches 15% due to the apparently enhanced ionic bond around Cr^{3+}. Moreover, the absorption bands of Cr^{3+}:$^4T_1$ and $^4T_2$ with different BaF_2 contents are illustrated in Fig. 3(d). The absorption intensity of Cr^{3+}:$^4T_1$ is constantly reduced and the peak center of Cr^{3+}:$^4T_2$ shows a blue shift when the amount of BaF_2 increases at 15%. According to the Ref. [28], it has been pointed out that this absorption band shift of Cr^{3+}:$^4T_2$ is attributed to the spin-orbit coupling between $^4T_2$, ^2E, $^2T_1$ excited states. When the content of BaF_2 reaches 15%, the overall excess of F^- and Ba^{2+} distinctly transforms the BaF_2 modified glass electronic structure where different spin multiplicities' states of Cr^{3+} are interacted [28].

Table 3 shows the absorption band positions, Racah parameters B and C, crystal-field parameter D_q/B of different Cr^{3+} doped glasses, which are calculated based on the absorption positions [12]. According to the Ref. [29] that $2.1 < D_q/B < 2.3$ distinguishes the low field from high field regions, D_q/B is slightly increased as BaF_2 content reaches 15%, which indicates that octahedral ligand field environment of Cr^{3+} is appropriately enhanced by fluorides [21]. Besides, on the basis of the $3d^3$ configuration given by Tanabe-Sugano diagram [12], the increased value of D_q/B is close to the crossing point among the field-independent ^2E, $^4T_2$, and $^2T_1$ energy curves [8]. Here, the anion type is changing as the substitution of BaF_2 is added, F^- possesses a

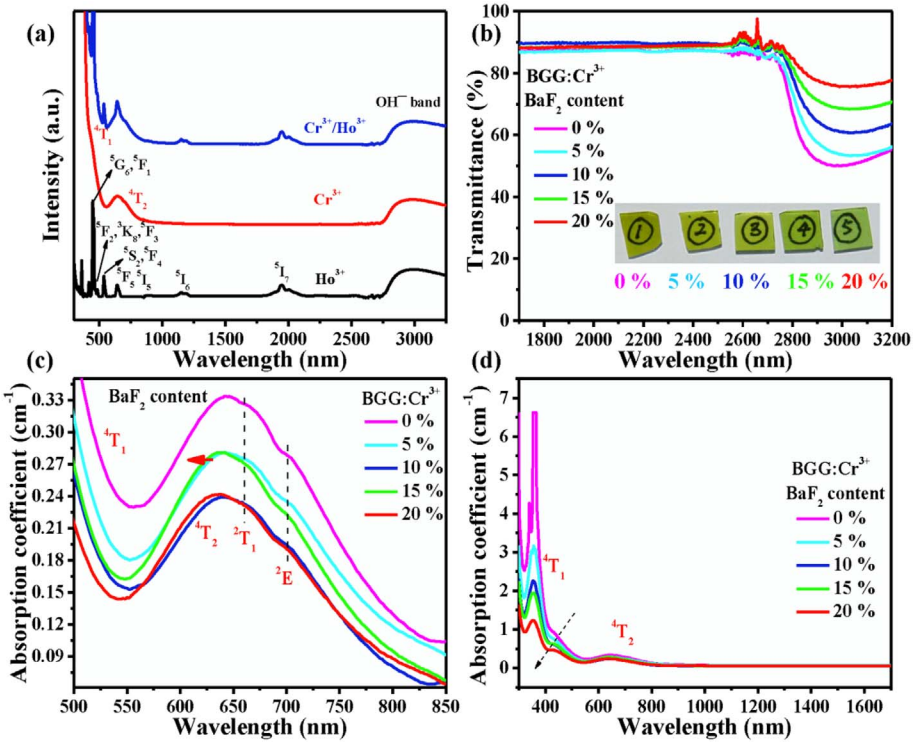

Fig. 3. (a) Absorption spectra of Cr^{3+}-, Ho^{3+}-, and Cr^{3+}/Ho^{3+} co-doped germanate glasses (b) transmission spectra of Cr^{3+}-doped glasses (c) zoomed $^4T_2$ absorption band and (d) absorption spectra of Cr^{3+}-doped glasses.

Table 3
Absorption band positions, Racah parameters B and C, crystal-field parameter D_q/B for Cr^{3+} in BGG:Cr^{3+} glasses with different BaF_2 contents and other glass hosts.

Glass	^2E (cm^{-1})	$^2T_1$ (cm^{-1})	$^4T_2$ (cm^{-1})	$^4T_1$ (cm^{-1})	B (cm^{-1})	C (cm^{-1})	D_q/B	Ref.
Fluoride	14,860	15,530	15,385	23,040	850	2948	1.84	[12]
Phosphate	14,660	15,870	15,270	22,370	756	3073	2.02	[12]
0%	14,354	15,249	15,527	23,026	815	2847	1.90	This work
5%	14,354	15,249	15,527	23,026	815	2847	1.90	
10%	14,354	15,249	15,527	23,026	815	2847	1.90	
15%	14,354	15,249	15,724	23,026	777	2921	2.02	
20%	14,354	15,249	15,724	23,026	777	2921	2.02	

Table 4
Comparison of J-O parameters Ω_t (t = 2, 4, 6) of Ho^{3+} ions in various glass hosts.

Glass	Ω_t ($\times 10^{-20}$ cm^2)			Ref.
	Ω_2	Ω_4	Ω_6	
Fluorophosphate	2.10	3.50	2.50	[33]
Gallate	5.70	3.10	0.37	[33]
Germanate	3.30	1.14	0.17	[33]
0%	5.75	3.18	0.92	This work
5%	5.62	3.11	0.90	
10%	5.53	3.06	0.89	
15%	5.42	3.00	0.87	
20%	5.35	2.96	0.86	

lower intensive electron density than O^{2-} does, and the larger value of D_q/B is assigned to the larger anion packing density [7].

Table 4 presents the Judd-Ofelt (J-O) parameters of Ho^{3+} doped various glasses [30,31]. Three parameters (Ω_t, t = 2, 4, 6) appear in the order of $\Omega_2 > \Omega_4 > \Omega_6$, here, Ω_2 is related to the hypersensitive transition. The large value of Ω_2 indicates the larger line strength of the hypersensitive transition and covalency parameter of rare-earth ions [32]. Monotonically dropped Ω_2 accordingly reveals the decreased covalency around Ho^{3+} ions. The Ho-F bond is more ionic than Ho-O bond due to the higher electronegativity of F (4.0) than O (3.44), which accounts for the constantly diminished Ω_2 as the amount of BaF_2 is added [26]. The rigidity of host glass is recommended by Ω_6, and the decreased Ω_6 indicates the reducing mechanical properties of glasses [26]. Based on the J-O parameters [32,33], the radiative transition probabilities (A_r), branching ratios (β), and radiative lifetimes (τ_r) of Ho^{3+} doped glasses are shown in Table 5. The value of A_r slightly decreases with adding the substitution of BaF_2. The A_r (81.0 s^{-1}) of 20% BaF_2 modified BGG:Cr^{3+}/Ho^{3+} sample is higher than that of germanate glass (39.7 s^{-1}) [33], and gallate glass (69.5 s^{-1}) [33]. Moreover, the radiative lifetimes (τ_r) of Ho^{3+}: $^5I_7 \rightarrow {}^5I_8$ transition are constantly prolonged with increasing the substitution of BaF_2 due to the reduced A_r [26]. The results demonstrate that Cr^{3+}/Ho^{3+} co-doped germanate glasses modified by a proper amount of BaF_2 can be comparatively a promising candidate to achieve 2.0 μm laser output.

Fig. 4 shows the near-infrared luminescent spectra of the BGG:Cr^{3+} with different BaF_2 contents pumped by Xe lamp at 619 nm and an 808 nm LD. The broad emissions around 878 and 1000 nm are enhanced with the substitution of BaF_2 added due to the diminished OH^- coefficient, both of them are attributed to Cr^{3+}: $^4T_2 \rightarrow {}^4A_2$ transition [7]. Meanwhile, Fig. 4(c) donates the normalized excitation spectra of Cr^{3+} monitored at 878 and 1000 nm. The similar excitation bands prove the same transitions from Cr^{3+}. Besides, this apparent shift of emission spectra of Cr^{3+} could be ascribed to the various excitation wavelengths of different powers and distinct photoresponse performances around the detection limit of the different detectors that R5509-72 PMT is for Xe lamp at 619 nm, InGaAs photoconductor for an 808 nm LD [7]. Besides, Fig. 4(d) donates the excitation spectra of Cr^{3+} doped glasses monitored at 878 nm with different amounts of BaF_2 added. The two broad bands around 450 and 650 nm are attributed to Cr^{3+}: $^4A_2 \rightarrow {}^4T_1$ and $^4A_2 \rightarrow {}^4T_2$ transitions, moreover, the sensitively detected centre positions of excitation bands are constantly blue-shifting due to the enhanced ionic bond as the electronegativity of F is larger than O.

Fig. 5(a) presents the near-infrared emission spectra of the BGG:Cr^{3+}/Ho^{3+} with different BaF_2 contents under the excitation of an 808 nm LD. The observed emissions can be divided into two bands around 1000 and 1200 nm, which are respectively attributed to Cr^{3+}: $^4T_2 \rightarrow {}^4A_2$ and Ho^{3+}: $^5I_6 \rightarrow {}^5I_8$ transitions. Besides, the lump around 1065 nm is contributed to the harmonic light of the high-powered 808 nm laser diode. In comparison with the Ho^{3+} doped glass, there is accordingly energy transfer from Cr^{3+} to Ho^{3+}:$^5I_6$ manifold. Besides, the radiative transitions of Cr^{3+} and Ho^{3+} are promoted by the substitution of BaF_2 due to the decreased OH^- coefficient. Fig. 5(b) illustrates the excitation spectra of the Ho^{3+} doped sample with different BaF_2 contents monitored at 1200 nm. The excited bands for Ho^{3+} are enhanced and broadened by Cr^{3+}, which originate from being singly

Table 5
The calculated electric dipole (A_{ed}) and magnetic dipole (A_{md}) transition probabilities, spontaneous radiative transition probabilities (A_r), branching ratios (β), and the radiative lifetimes (τ_r) in BGG:Cr^{3+}/Ho^{3+} with different BaF_2 contents.

Sample	Initial state	Final state	A_{ed} (s^{-1})	A_{md} (s^{-1})	A_r (s^{-1})	β (%)	τ_r (ms)
0%	$^5I_7$	$^5I_8$	60.24	31.77	92.01	100	10.87
	$^5I_6$	$^5I_8$	131.50		131.50	80.80	
		$^5I_7$	15.22	16.04	31.26	19.20	6.14
5%	$^5I_7$	$^5I_8$	58.58	31.60	90.18	100	11.09
	$^5I_6$	$^5I_8$	127.87		127.87	80.61	
		$^5I_7$	14.80	15.96	30.75	19.39	6.30
10%	$^5I_7$	$^5I_8$	55.60	30.51	86.10	100	11.61
	$^5I_6$	$^5I_8$	121.41		121.41	80.49	
		$^5I_7$	14.03	15.40	29.44	19.51	6.63
15%	$^5I_7$	$^5I_8$	53.75	30.18	83.93	100	11.91
	$^5I_6$	$^5I_8$	117.35		117.35	80.29	
		$^5I_7$	13.57	15.24	28.81	19.71	6.84
20%	$^5I_7$	$^5I_8$	51.64	29.43	81.08	100	12.33
	$^5I_6$	$^5I_8$	112.77		112.77	80.17	
		$^5I_7$	13.04	14.86	27.90	19.83	7.11

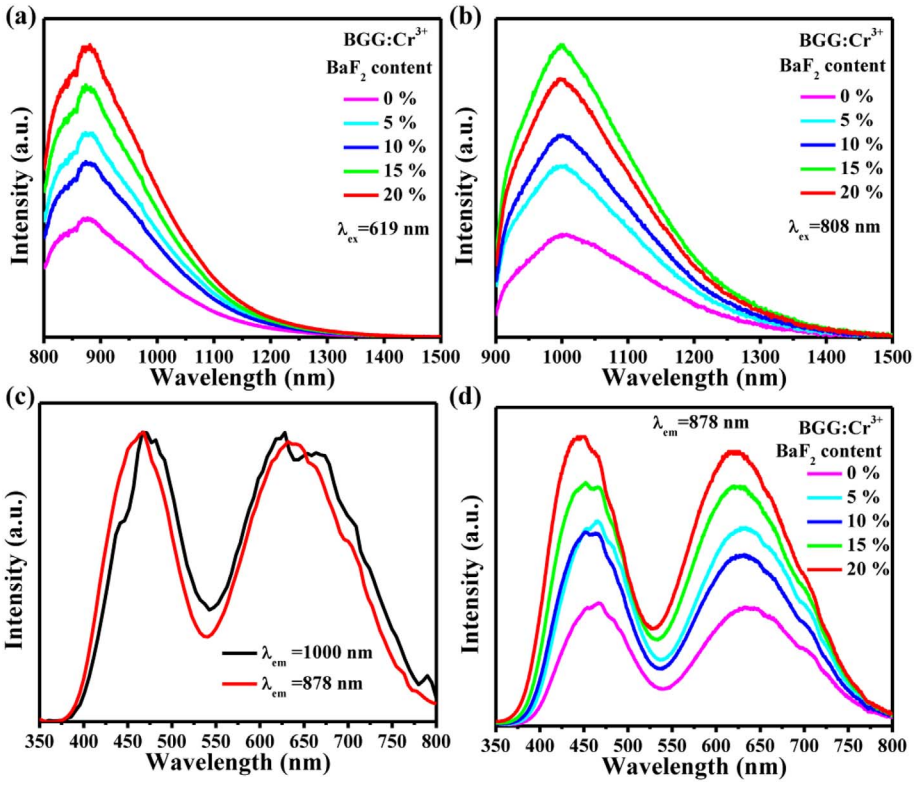

Fig. 4. Emission spectra upon the excitation of (a) Xe lamp at 619 nm and (b) 808 nm LD, (c) normalized excitation spectra monitored at 878 nm and 1000 nm or (d) monitored at 878 nm in Cr^{3+}-doped glasses with different BaF_2 contents.

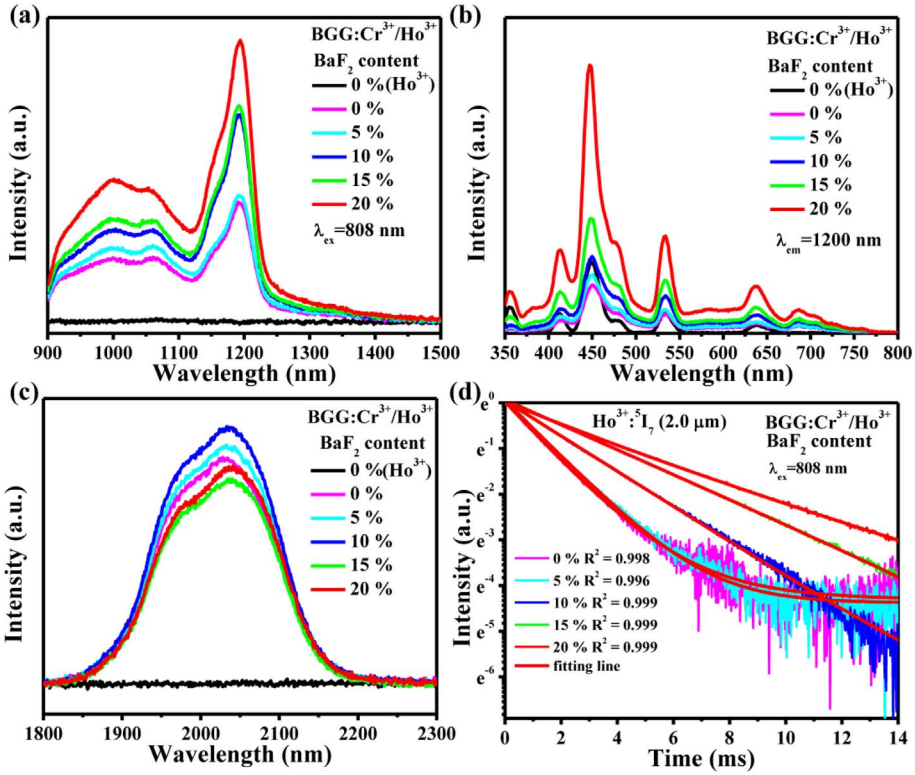

Fig. 5. (a) Near-infrared emission spectra (b) excitation spectra (c) mid-infrared emission spectra and (d) decay curves in Cr^{3+}/Ho^{3+} co-doped glasses.

confined to widely broadened ranging from 350 nm near to 800 nm. This signifies energy transfer(ET) from Cr^{3+} to Ho^{3+} and a large range of pump sources is expected to be applied. Besides, there are different phenomena of the excitation positions of Cr^{3+} and Ho^{3+} influenced by adding BaF_2. The sensitive *d-d* transitions of Cr^{3+} distinctly move towards the short wavelength, however, the *f-f* transition manifolds of Ho^{3+} are mainly confined and populated by Cr^{3+}. Fig. 5(c–d) demonstrates the luminescent spectra and the decay curves of 2.0 μm emissions in the BGG:Cr^{3+}/Ho^{3+} with different BaF_2 contents. The emission band of 2.0 μm is attributed to Ho^{3+}: $^5I_7 \rightarrow {}^5I_8$ transition. The largest fluorescence intensity is located at the 10% amount of BaF_2 modified sample. The result indicates that the proper amount of BaF_2 is

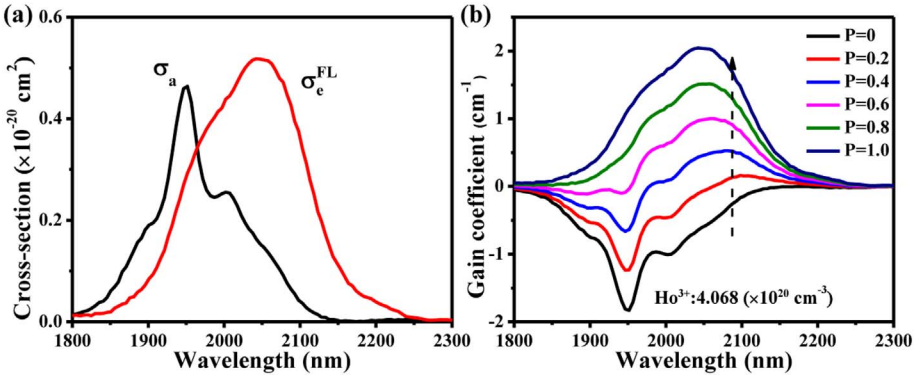

Fig. 6. (a) The absorption and emission cross-sections (b) estimated gain coefficients corresponding to Ho^{3+}: $^5I_7 \rightarrow {}^5I_8$ transition in BGG:Cr^{3+}/Ho^{3+} with 10% BaF_2 content.

Table 6
Spectroscopic properties of Ho^{3+}:$^5I_7$ level in BGG:Cr^{3+}/Ho^{3+} with 10% BaF_2 content and other glasses.

Glass	Ho^{3+} ions (10^{20} cm^{-3})	λ (nm)	τ_m (ms)	FWHM (nm)	σ_e^{FL} (10^{-21} cm^2)	FWHM × σ_e^{FL} (10^{-26} cm^2)	Ref.
Fluoride	2	2035	26.70	118	5.3	6.25	[33]
Silicate	2	2040	0.32	82	7.0	5.74	[33]
Germanate	2	2045	0.36	84	4.0	3.36	[33]
Fluorophosphate	2	2035	5.60	123	7.9	9.72	[33]
10%	4	2047	2.57	175	5.2	9.10	This work

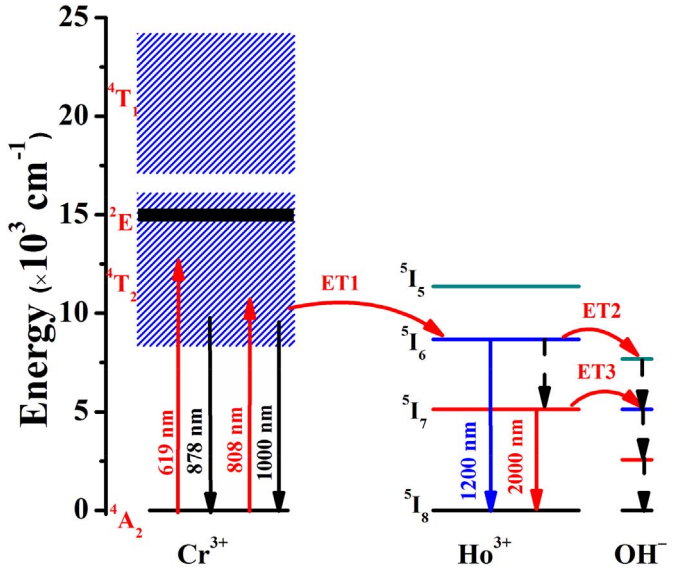

Fig. 7. Simplified energy diagram of Cr^{3+}/Ho^{3+} co-doped glass as well as the quenching effect of OH^-.

Table 7
Calculated non-radiative probabilities of Ho^{3+}:$^5I_7$ level for different amounts of BaF_2 modified samples and other glasses.

Sample	ZBLAN	Silicate	0%	5%	10%	15%	20%
W_{nr} (s^{-1})	4	359	562	531	303	197	151
Ref.	[37]	[38]	This work				

10%. Besides, the measured lifetimes (τ_m) of 2.0 μm are determined as 1.53 ms, 1.61 ms, 2.57 ms, 3.56 ms, 4.31 ms, increased with the substitution of BaF_2 added due to the diminished quenching center of OH^- groups.

The absorption ($\sigma_a(\lambda)$) and emission ($\sigma_e^{FL}(\lambda)$) cross-sections of Ho^{3+}:2.0 μm are respectively determined by the Lambert-Beer law and Fuchtbauer-Ladenburg (FL) equation [32], as depicted in Fig. 6(a). The $\sigma_a(\lambda)$ of Ho^{3+}: $^5I_8 \rightarrow {}^5I_7$ transition in BGG:Cr^{3+}/Ho^{3+} with 10% amount of BaF_2 is calculated as 4.6×10^{-21} cm^2 at 1950 nm, $\sigma_e^{FL}(\lambda)$ is 5.2×10^{-21} cm^2 at 2047 nm, and FWHM is as wide as 175 nm. Meanwhile, FWHM × $\sigma_e^{FL}(\lambda)$ is an important parameter for estimating gain properties, the larger value generally represents a wider bandwidth and a higher gain character. Table 6 displays the spectroscopic properties of Ho^{3+} near 2.0 μm in different glass hosts, and our sample has an advantage among the others. Fig. 6(b) shows the gain cross-section spectra ($G(\lambda)$) of BGG:Cr^{3+}/Ho^{3+} with 10% amount of BaF_2, which is computed by $G(\lambda) = N \times [P \times \sigma_e^{FL}(\lambda) - (1 - P) \times \sigma_a(\lambda)]$ [26], where P is the population inversion given by the population ratio among the upper and lower manifolds. N is the calculated ion concentration of Ho^{3+} and determined as 4.068×10^{20} cm^{-3}. With varying a set of P values from 0 to 1, the gain cross-section spectra are calculated and depicted *versus* the wavelength. Obviously, when P is at around 0.4, the positive gain occurs. The maximum gain coefficient of Ho^{3+}: $^5I_7 \rightarrow {}^5I_8$ transition is 2.06 cm^{-1}, which is larger than that of some lead silicate glasses (0.89 cm^{-1}) [34], fluorophosphate glasses (0.74 cm^{-1}) [35], and silica-germanate glass (1.9 cm^{-1}) [36].

Based on the above results and Tanabe-Sugano diagram [12], a possible energy transfer mechanism [7,26] between Cr^{3+} and Ho^{3+} ions is illustrated in Fig. 7. The effects of spin-orbit coupling and electron-vibration interaction mix the $^4T_2$ and ^2E levels together [8]. The ^2E level separates the 619 and 808 nm pump channels due to the energy difference. Populations on Cr^{3+}:$^4A_2$ state are initially pumped to the $^4T_2$ state, then ions on the $^4T_2$ decay to the $^4A_2$ state with 878 and 1000 nm emissions under the excitations of Xe lamp at 619 nm or an 808 nm LD, respectively. Furthermore, ions on the $^4T_2$ manifold are derived from the $^4A_2$ state *via* the excitations of 619 or 808 nm pump sources, then the energy transfers (ET1: Cr^{3+}:$^4T_2$ + Ho^{3+}:$^5I_8 \rightarrow Cr^{3+}$:$^4A_2$ + Ho^{3+}:$^5I_6$) to the adjacent Ho^{3+}:$^5I_6$ state [7] after the addition of Ho^{3+}. The ions on the $^5I_6$ state degenerate to the $^5I_8$ ground manifold with 1200 nm emission or non-radiatively decay to the $^5I_7$ state quenched by OH^- groups (ET2: Ho^{3+}:$^5I_6 \rightarrow OH^-$). Meanwhile, ions on the $^5I_7$ manifold decay to the $^5I_8$ state with delivering 2.0 μm emission, partly depopulate to the OH^- groups (ET3: Ho^{3+}:$^5I_7 \rightarrow OH^-$). As the amount of BaF_2 is monotonously added, the OH^- coefficient is lowered and the energy transfers from Ho^{3+}:$^5I_6$ or $^5I_7$ and Cr^{3+}:$^4T_2$ to OH^- groups are suppressed, which is beneficial for near and mid-infrared luminescence. Based on the measured lifetimes (τ_m) and calculated radiative lifetimes (τ_r) of Ho^{3+}:2.0 μm, the non-radiative probability W_{nr} of the $^5I_7$ level can be obtained by $W_{nr} = 1/$

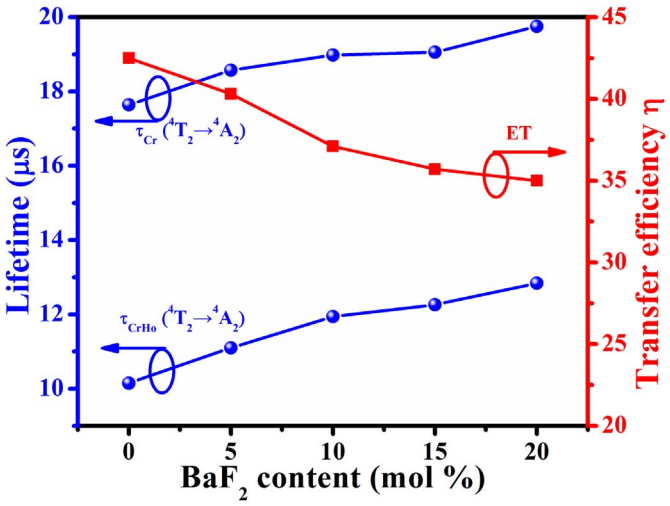

Fig. 8. The average luminescent lifetime of Cr^{3+}:$^4T_2$ monitored at 878 nm upon excitation of 619 nm as well as the related energy transfer efficiency η from Cr^{3+} to Ho^{3+}.

$\tau_m - 1/\tau_r$ [26], the calculated results are provided at Table 7. The W_{nr} of the $^5I_7$ level in fluorozirconate glass (ZBLAN) is quite low [37] due to its low maximum phonon energy and low OH^- coefficient. And after 20% BaF_2 is added, the W_{nr} of the germanate glass is lower than that of silicate glass (359 s^{-1}) [38]. The constantly decreased W_{nr} indicates the diminished OH^- coefficient is favor of the radiative transition of Ho^{3+}:$^5I_7$, and thus a BaF_2 modified germanate glass may have promising value as a material for a laser at 2.0 μm [39].

Fig. 8 depicts the average luminescent lifetimes of Cr^{3+}:$^4T_2$ state in Cr^{3+} (τ_{Cr}) doped and Cr^{3+}/Ho^{3+} (τ_{CrHo}) co-doped glasses with different BaF_2 contents. The average lifetimes of Cr^{3+}: $^4T_2 \rightarrow {}^4A_2$ (878 nm) are prolonged with the substitution of BaF_2 added due to lowered OH^- coefficient, and the lifetime of Cr^{3+} doped sample is enhanced as long as 19.75 μs by the fluorides, which is much longer than that of alkali silicate glasses (~10 μs) [11]. The transfer efficiency (η) is calculated by $\eta = 1 - \tau_{Cr}/\tau_{CrHo}$ [40]. The achieved η of $Cr^{3+} \rightarrow Ho^{3+}$ varies with BaF_2 contents and reaches as high as 42.5% without BaF_2, which is higher than that of fluorogermanate glasses (26.2%) [7] and similar to that of Yb^{3+} (42.6%) [41]. All results indicate the Cr^{3+} ion could be a good sensitizer for Ho^{3+}.

4. Conclusion

In summary, an enhanced 2.0 μm emission of Cr^{3+}/Ho^{3+} co-doped germanate glass modified by BaF_2 is achieved under an 808 nm LD excitation. The addition of BaF_2 can distinctly diminish the refractive index and density of glass samples, furthermore, the OH^- coefficient is reduced as low as 1.08 cm^{-1} that is responsible for the promoted emission intensity and lifetime of Cr^{3+} and Ho^{3+} activators. Attractively, the excitation spectra of Cr^{3+} can be easily tailored by the incorporation of BaF_2, which ultimately makes a higher pump efficiency for achieving an efficient energy transfer process from Cr^{3+} to Ho^{3+}. An even more rewarding result is that the energy transfer efficiency from Cr^{3+} to Ho^{3+} is improved as high as 42.5% due to the suppressed non-radiative probability of $^5I_7$ level by the substitution of BaF_2. These results suggest that Cr^{3+}/Ho^{3+} doped germanate glass modified by BaF_2 can be considered as a boosted candidate for efficient 2.0 μm fiber lasers operated at various pump sources.

Acknowledgments

This work is financially supported by the National Science Foundation of China (Grants Nos. U1601205 and 51472088). Decay lifetime measurements are supported by Z.Y. Zhao from State Key Laboratory of Silicate Materials for Architectures, Wuhan University of Technology.

References

[1] L.X. Li, W.C. Wang, C.F. Zhang, J. Yuan, B. Zhou, Q.Y. Zhang, Opt. Mater. Express 6 (2016) 2904–2914.
[2] Z.J. Xing, S. Gao, X.Q. Liu, S.Y. Sun, C.L. Yu, L.M. Xiong, K.F. Li, M.S. Liao, J. Alloys Compd. 660 (2016) 375–381.
[3] J.T. Fan, Y.Y. Fan, Y. Yang, D.P. Chen, L. Calveza, X.H. Zhang, L. Zhang, J. Non-Cryst. Solids 357 (2011) 2431–2434.
[4] Y. Tian, X.F. Jing, S.Q. Xu, Spectrochim. Acta A 115 (2013) 33–38.
[5] T. Wei, Y. Tian, C. Tian, M.Z. Cai, X.F. Jing, B.P. Li, R. Chen, J.J. Zhang, S.Q. Xu, J. Phys. Chem. A 119 (2015) 6823–6830.
[6] J. Yuan, S.X. Shen, D.D. Chen, Q. Qian, M.Y. Peng, Q.Y. Zhang, J. Appl. Phys. 113 (2013) 173507.
[7] F.F. Zhang, J. Yuan, Y. Liu, W.C. Wang, D.C. Yu, M.Y. Peng, Q.Y. Zhang, Opt. Mater. Express 4 (2014) 1404–1410.
[8] W.C. Wang, J. Yuan, D.D. Chen, J.J. Zhang, S.Q. Xu, Q.Y. Zhang, AIP Adv. 4 (2014) 107145.
[9] W.C. Wang, Q.H. Le, Q.Y. Zhang, L. Wondraczek, J. Mater. Chem. C 5 (2017) 7969–7976.
[10] F. Rasheed, K.P.O. Donnell, B. Henderson, D.B. Hollis, J. Phys. Condens. Matter 3 (1991) 3825–3840.
[11] U.R. Rodriguez-Mendoza, V.D. Rodriguez, I.R. Martin, V. Lavin, J. Mendez-Ramos, P. Nunez, J. Alloys Compd. 323 (2001) 759–762.
[12] M. Yamaga, B. Henderson, K.P.O. Donnell, Y. Gao, Phys. Rev. B 44 (1991) 4853–4861.
[13] R. Lachheb, A. Herrmann, K. Damak, C. Rüssel, R. Maâlej, J. Lumin. 186 (2017) 152–157.
[14] D.C. Zhou, X.M. Bai, H. Zhou, Sci. Rep. 7 (2017) 44747.
[15] R.J. Cao, Y. Lu, Y. Tian, F.F. Huang, Y.Y. Guo, S.Q. Xu, J.J. Zhang, Sci. Rep. 6 (2016) 37873.
[16] F.F. Huang, X.Q. Liu, Y. Zhang, L.L. Hu, D.P. Chen, Opt. Lett. 39 (2014) 5917–5920.
[17] D.H. Li, W.B. Xu, P.W. Kuan, W.T. Li, Z.Q. Lin, X. Wang, L. Zhang, C.L. Yu, K.F. Li, L.L. Hu, Ceram. Int. 42 (2016) 10493–10497.
[18] H. Hosono, Y. Abe, J. Am. Ceram. Soc. 72 (1989) 44–48.
[19] J.T. Fan, B. Tang, W. Dong, Y.Y. Fan, R.H. Li, J.C. Li, D.P. Chen, L. Calveza, X.H. Zhang, L. Zhang, J. Non-Cryst. Solids 357 (2011) 1106–1109.
[20] L. Zur, J. Janek, M. Soltys, T. Goryczka, J. Pisarska, W.A. Pisarski, J. Non-Cryst. Solids 431 (2016) 145–149.
[21] S.Q. Zhang, M.X. Xu, X. Chen, Y.L. Zhang, L. Calvez, X.H. Zhang, Y.S. Xu, Y. Huai, Y.Q. Jin, J. Am. Ceram. Soc. 96 (2013) 2461–2466.
[22] P.L. Higby, I.D. Aggarwal, J. Non-Cryst. Solids 163 (1993) 303–308.
[23] Z.H. Jiang, Q.Y. Zhang, Sci. China Mater. 58 (2015) 378–425; Z.H. Jiang, Q.Y. Zhang, Prog. Mater. Sci. 61 (2014) 144–215.
[24] J. Yuan, S.X. Shen, W.C. Wang, M.Y. Peng, Q.Y. Zhang, Z.H. Jiang, J. Appl. Phys. 114 (2013) 133506.
[25] H.F. Chen, F.Z. Chen, T. Wei, Q.H. Liu, R.X. Shen, Y. Tian, Opt. Commun. 321 (2014) 183–188.
[26] F.F. Zhang, W.J. Zhang, J. Yuan, D.D. Chen, Q. Qian, Q.Y. Zhang, AIP Adv. 4 (2014) 047101.
[27] X. Wen, G.W. Tang, J.W. Wang, X.D. Chen, Q. Qian, Z.M. Yang, Opt. Express 23 (2015) 7722–7731.
[28] O. Maalej, O. Taktak, B. Boulard, S. Kammoun, J. Phys. Chem. B 120 (2016) 7538–7545.
[29] D.L. Russell, K. Holliday, M. Grinberg, D.B. Hollis, Phys. Rev. B 59 (1999) 13712–13718.
[30] B.R. Judd, Phys. Rev. 127 (1962) 750–761.
[31] G.S. Ofelt, J. Chem. Phys. 37 (1962) 511–520.
[32] G.X. Chen, Q.Y. Zhang, G.F. Yang, Z.H. Jiang, J. Fluoresc. 17 (2007) 301–307.
[33] B. Peng, T. Izumitani, Opt. Mater. 4 (1995) 797–810.
[34] T.T. Zhu, G.W. Tang, X.D. Chen, M. Sun, Q. Qian, D.D. Chen, Z.M. Yang, Int. J. Appl. Glas. Sci. 8 (2017) 196–203.
[35] Y. Tian, L.Y. Zhang, S.Y. Feng, R.R. Xu, L.L. Hu, J.J. Zhang, Opt. Mater. 32 (2010) 1508–1513.
[36] T. Wang, F.F. Huang, W.Q. Cao, Y.Y. Guo, R.S. Lei, R.G. Ye, J.J. Zhang, S.Q. Xu, Opt. Mater. Express 7 (2017) 1084–1095.
[37] L. Wetenkamp, G.F. West, H. Többen, J. Non-Cryst. Solids 140 (1992) 35–40.
[38] X. Wang, X.K. Fan, S. Gao, K.F. Li, L.L. Hu, Ceram. Int. 40 (2014) 9751–9756.
[39] R. Reisfeld, J. Hormadaly, A. Muranevich, J. Non-Cryst. Solids 29 (1978) 323–332.
[40] W.C. Wang, J. Yuan, X.Y. Liu, D.D. Chen, Q.Y. Zhang, Z.H. Jiang, J. Non-Cryst. Solids 404 (2014) 19–25.
[41] L.L. Tao, Y.H. Tsang, B. Zhou, B. Richards, A. Jha, J. Non-Cryst. Solids 358 (2012) 1644–1648.